AIP | Applied Physics Letters

Ultraviolet surface plasmon-mediated low temperature hydrazine decomposition

Siying Peng, Matthew T. Sheldon, Wei-Guang Liu, Andres Jaramillo-Botero, William Andrew Goddard III, and Harry A. Atwater

Citation: Applied Physics Letters **106**, 023102 (2015); doi: 10.1063/1.4905593
View online: http://dx.doi.org/10.1063/1.4905593
View Table of Contents: http://scitation.aip.org/content/aip/journal/apl/106/2?ver=pdfcov
Published by the AIP Publishing

Articles you may be interested in

High-performance AlGaN metal–semiconductor–metal solar-blind ultraviolet photodetectors by localized surface plasmon enhancement
Appl. Phys. Lett. **106**, 021112 (2015); 10.1063/1.4905929

Strong coupling between Rhodamine 6G and localized surface plasmon resonance of immobile Ag nanoclusters fabricated by direct current sputtering
Appl. Phys. Lett. **102**, 143112 (2013); 10.1063/1.4801633

Sensing properties of infrared nanostructured plasmonic crystals fabricated by electron beam lithography and argon ion milling
J. Vac. Sci. Technol. B **30**, 06FE02 (2012); 10.1116/1.4767274

Tailoring plasmon resonances in the deep-ultraviolet by size-tunable fabrication of aluminum nanostructures
Appl. Phys. Lett. **101**, 081110 (2012); 10.1063/1.4747489

Molded plasmonic crystals for detecting and spatially imaging surface bound species by surface-enhanced Raman scattering
Appl. Phys. Lett. **94**, 243109 (2009); 10.1063/1.3155198

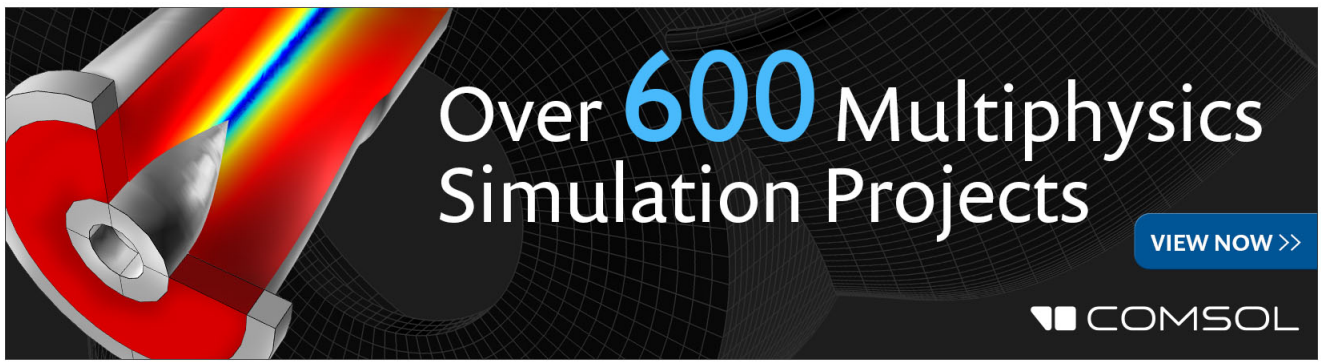

This article is copyrighted as indicated in the article. Reuse of AIP content is subject to the terms at: http://scitation.aip.org/termsconditions. Downloaded to IP: 131.215.70.231 On: Tue, 20 Jan 2015 15:53:04

Ultraviolet surface plasmon-mediated low temperature hydrazine decomposition

Siying Peng (彭斯颖),[1] Matthew T. Sheldon,[1] Wei-Guang Liu,[2] Andres Jaramillo-Botero,[2] William Andrew Goddard III,[2] and Harry A. Atwater[1]
[1]*Thomas J. Watson Laboratories of Applied Physics, California Institute of Technology, Pasadena, California 91125, USA*
[2]*Materials and Process Simulation Center, California Institute of Technology, Pasadena, California 91125, USA*

(Received 27 August 2014; accepted 26 December 2014; published online 12 January 2015)

Conventional methods require elevated temperatures in order to dissociate high-energy nitrogen bonds in precursor molecules such as ammonia or hydrazine used for nitride film growth. We report enhanced photodissociation of surface-absorbed hydrazine (N_2H_4) molecules at low temperature by using ultraviolet surface plasmons to concentrate the exciting radiation. Plasmonic nanostructured aluminum substrates were designed to provide resonant near field concentration at $\lambda = 248$ nm (5 eV), corresponding to the maximum optical cross section for hydrogen abstraction from N_2H_4. We employed nanoimprint lithography to fabricate 1 mm × 1 mm arrays of the resonant plasmonic structures, and ultraviolet reflectance spectroscopy confirmed resonant extinction at 248 nm. Hydrazine was cryogenically adsorbed to the plasmonic substrate in a low-pressure ambient, and 5 eV surface plasmons were resonantly excited using a pulsed KrF laser. Mass spectrometry was used to characterize the photodissociation products and indicated a 6.2× overall enhancement in photodissociation yield for hydrazine adsorbed on plasmonic substrates compared with control substrates. The ultraviolet surface plasmon enhanced photodissociation demonstrated here may provide a valuable method to generate reactive precursors for deposition of nitride thin film materials at low temperatures. © *2015 AIP Publishing LLC*. [http://dx.doi.org/10.1063/1.4905593]

Gallium nitride (GaN) and indium gallium nitride (InGaN) are tunable wide band gap semiconductor materials with important applications in optoelectronic devices such as LEDs and photovoltaics.[1,2] Conventional growth methods for these materials include chemical vapor deposition (CVD) and molecular beam epitaxy (MBE), which both require high temperatures (>500 K) to create atomic nitrogen growth species by thermal decomposition of nitride precursor molecules.[3] Alternatively, magnetron sputtering can be used to grow nitride semiconductors at room temperature.[4] However, the sputtering process utilizes high-energy plasma ions to bombard nitride precursors, resulting in a high kinetic energy distribution of atomic nitrogen that limits the crystalline quality of the growing film. By contrast, ultraviolet (UV) radiation can resonantly dissociate nitrogen bonds, through a pathway that does not produce species with high kinetic energy or require high temperatures. By generating a kinetic energy distribution of the dissociated nitrogen species similar to that achieved in molecular beam epitaxy or chemical vapor deposition processes, resonant ultraviolet dissociation of nitrogen precursors may enable low temperature film growth with superior crystalline quality. Additionally, because film growth could occur at lower temperatures, such a process may open doors for synthesis of difficult-to-make semiconductor materials such as indium rich InGaN, which is normally hindered due to phase separation into InN and GaN at elevated growth temperatures.[5,6]

We utilize the optical confinement properties of surface plasmons to localize ultraviolet radiation in a surface-adsorbed hydrazine layer and thus generate a high flux of reactive nitrogen species athermally, with the aim of overcoming the limitations of conventional high temperature nitride film growth, a method of nitride precursor generation that has not been demonstrated before. Surface plasmons are coherent oscillations of charge density at the interface of a metal and a dielectric that confine incident radiation within evanescent fields of subwavelength extent in the direction perpendicular to the surface, thereby providing concentration of optical intensity at resonance up to 1000× greater than the free space intensity in some cases.[7] This remarkable property of surface plasmons has been studied extensively for various applications such as surface-enhanced Raman scattering (SERS),[8] surface enhanced photo-chemistry,[9–15] optical tweezing,[16] and nanoparticle therapeutics.[17] In our experiment, the enhancement of radiation fields via surface plasmon excitation is employed to maximize resonant ultraviolet decomposition of nitride growth precursor molecules that are cryogenically condensed at high concentration on plasmonically active substrates.

We identify hydrazine (N_2H_4) as a promising nitride growth precursor molecule for low temperature film growth. N_2H_4 molecules have a dissociation threshold at $\lambda = 376.2$ nm and very large optical absorption cross section at 5 eV ($\lambda = 248$ nm),[18,19] which is compatible with an KrF excimer laser excitation at 248 nm. Figure 1 shows the potential energy diagram along the N-H bond in a N_2H_4 molecule calculated at the level of GVB-RCI (generalized valence bond - restricted configuration interaction) (restricted double excitation)[20]/cc-pVTZ//B3LYP/6–311++G**. Optical excitation at 5 eV resonantly excites the N-H bond in the singlet electronic ground state (S_0) which we calculated to have an energy barrier of 4.0 eV after including the zero point energy correction, from a lower roto-vibrational state to a higher roto-vibrational

 © 2015 AIP Publishing LLC

This article is copyrighted as indicated in the article. Reuse of AIP content is subject to the terms at: http://scitation.aip.org/termsconditions. Downloaded to IP: 131.215.70.231 On: Tue, 20 Jan 2015 15:53:04

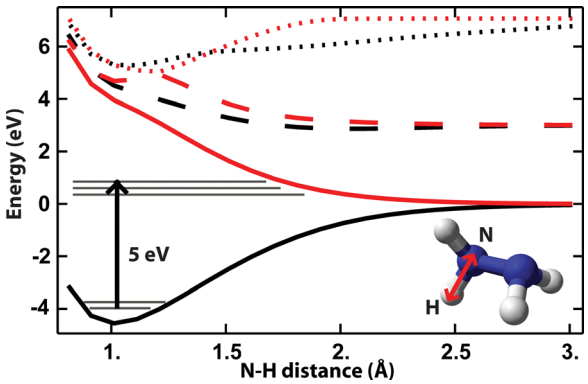

FIG. 1. N_2H_4 energy curve: Solid black curve (S_0) is the singlet ground state for the N-H bond. Inside the potential well of S_0, the horizontal lines represent the roto-vibrational states. Optical excitation at 5 eV (free space wavelength 248 nm) excites the ground state to higher roto-vibrational states and dissociates the N-H bond. The calculated curves depict the triplet first excited state (T_1, solid red), the singlet first excited state (S_1, dash black), the triplet second excited state (T_2, dashed red), the singlet second excited state (S_2, dotted black), and the triplet third excited state (T_3, dotted red).

state. The higher roto-vibrational state is sufficiently energetic to overcome the potential well of the S_0 state, resulting in the stretch of the N-H bond and ultimately, bond dissociation, and energizing other degree of freedoms in the molecule with the excess energy from the surface plasmon (1.0 eV in this case). We note that the energy gap between the ground state S_0 and the first excited state T_1 is 8.6 eV, which is too large to be excited by a 5 eV surface plasmon. We utilize surface plasmons to enhance the ultraviolet radiation field that excites the 5 eV dissociation pathway in N_2H_4. Ultraviolet surface plasmons have been studied in the past to enhance surface photochemical reactions,[9] increase sensitivity of SERS,[8] and generate photoelectron emission.[21] In the above context, aluminum has been identified as a promising ultraviolet plasmonic material for two reasons: its high bulk plasmon energy in the deep ultraviolet and low optical loss[21–23] entails that it provides strong ultraviolet field enhancement compared to more conventional plasmonic materials such as gold and silver.

To optimize plasmonic concentration of optical energy at 5 eV and facilitate dissociation of N_2H_4, we performed full wave electromagnetic simulations of surface plasmon modes in aluminum nanostructures. We identified a periodic aluminum grating structure as a simple and promising geometry, because it enables momentum matching between incident photons and surface plasmon modes on the metal. Shown in Figure 2(a) is the modeled reflectance over energy and wave number $k_g = (\frac{2\pi}{grating\ pitch})$, of an aluminum grating where a 4 nm native oxide on the surface (shown in Figure 2(b)) is included in the model. The width of the ridges (W in Figure 2(b)) of the grating increases as the grating pitch increases. Both the photonic dispersion and surface plasmon dispersion are manifested as a valley in reflectance spectrum (blue color in Figure 2(a)), indicated by the dashed lines. At lower wavenumber (larger pitch), the surface plasmon approaches the light line. As the wavenumber increases, the surface plasmon diverges from the light line and approaches an asymptotic limit, indicating localization of the optical field on the surface of the aluminum. In Figure 2(a), the reflectance valley indicated by the circles arises from the localized surface plasmon

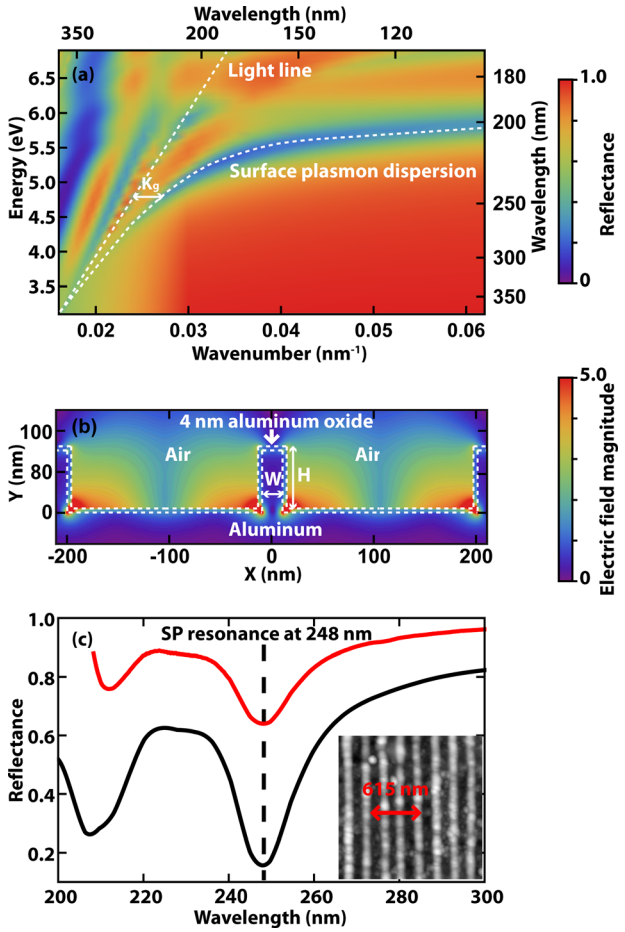

FIG. 2. (a) Full wave (finite-difference time-domain) simulation of the reflectance versus wavenumber, $k_g = (\frac{2\pi}{grating\ pitch})$, and energy of the aluminum grating with 4 nm aluminum oxide on top. The surface plasmon dispersion and the photon dispersion are manifested as the reflectance minimums (dashed white) in the density plot. Localized surface plasmon modes (circles) and photonic modes (stars) are also indicated. (b) The electric field magnitude for two grating periods of the optimized design, with 248 nm incident photons, shows strong field confinement near the surface. The aluminum grating and aluminum oxide layers are marked by white dotted lines. (c) Full wave simulation (FDTD) of the reflectance spectrum at normal incidence is shown (black). The red curve is the experimentally measured reflectance. The dip in reflectance in both the simulated and measured spectra indicates a surface plasmon resonance at 248 nm. Inset: AFM image of the fabricated grating.

mode at the ridges of the grating. Similar to the localized plasmonic mode of a metal nanoparticle, the energy of this localized surface plasmon mode decreases as W increases with the grating pitch. The broader reflectance valley at small wavenumber indicated by the stars corresponds to photonic modes and reveals the diffraction orders of the aluminum grating. We performed a systematic parameter variation changing W, the grating height (H in Figure 2(b)), and pitch of the grating to determine the geometry with minimum reflectance at 248 nm, corresponding to maximum field concentration in the plasmonic mode. We observe the strongest surface plasmon resonance at this wavelength for a grating period of 205 nm, width of 24 nm, and height of 50 nm. The electric field magnitude of the optimal geometry (Figure 2(b)) indicates that the optical energy is clearly confined close to the surface of the metal. By integrating of the electric field magnitude, we observe a near-field enhancement factor of 25× in the optimized design.

This article is copyrighted as indicated in the article. Reuse of AIP content is subject to the terms at: http://scitation.aip.org/termsconditions. Downloaded to IP: 131.215.70.231 On: Tue, 20 Jan 2015 15:53:04

A large area aluminum grating structure with the optimized design identified above was fabricated using a nanoimprint lithography process in which electron beam lithography was used to fabricate the nanoimprint stamp.[24] Briefly, electron beam lithography was used to pattern a silicon wafer coated with negative resist. A grating pattern was etched into the silicon wafer via reactive plasma etching (C_4F_8 and SF_6). The pattern on the silicon wafer was then transferred into a stamp of high modulus polymethyl disiloxane (PDMS). The transferred pattern was stamped into a sol-gel silica film spun onto a sputtered aluminum film via soft contact with the high modulus PDMS stamp. A reactive plasma etch (Cl_2 and HBr) was then performed to transfer patterns from the silica into the aluminum film. An atomic force microscope (AFM) image of the fabricated aluminum grating is shown as the inset of Figure 2(c). The total area of the patterned structure is 1 mm × 1 mm, and the average period is 205 nm, with an average grating width of 24 nm.

We measured the ultraviolet reflectance (Figure 2(c)) of the fabricated aluminum grating using an integrating sphere purged with nitrogen, in order to minimize ultraviolet absorption by atmospheric oxygen. The ultraviolet source of the integrating sphere illuminates the sample at an angle of 8° relative to normal incidence. In experiments that utilize the grating to dissociate N_2H_4, described below (Figure 3), a 248 nm excimer laser excites the grating at normal incidence. However, the surface plasmon resonance of the grating is highly dependent on incident angle, so the measured reflectance spectrum, taken at 8° incidence, has been transformed mathematically to depict the reflectance at normal incidence in order to better compare with experimental conditions. The measured spectrum after this transformation is shown as the red curve in Figure 2(c). In both the measured and simulated (black) reflectance spectrum, a surface plasmon resonance at 248 nm is clearly visible. The difference in reflectance between the experimentally measured spectrum and the simulated spectrum is attributed to defects in the fabricated aluminum grating.

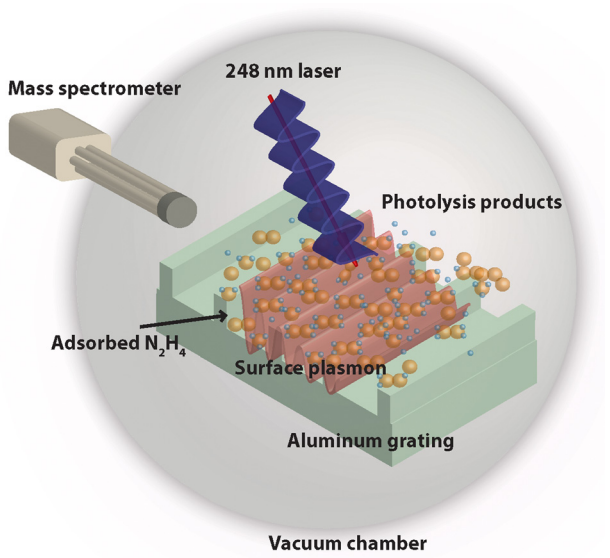

FIG. 3. Schematic illustration of ultraviolet surface plasmon mediated athermal resonant dissociation of N_2H_4. A 248 nm laser at normal incidence excites ultraviolet surface plasmons on the surface of a nanostructured Al grating which has been cooled to 77 K inside a low pressure atmosphere of N_2H_4 (10^{-5} Torr). The localized optical field resonantly dissociates N_2H_4 molecules adsorbed to the grating surface, and the dissociated species are detected via mass spectrometry.

To experimentally characterize the efficiency of the ultraviolet surface plasmon mediated dissociation of N_2H_4, we utilize mass spectrometry measurements of surface desorbed species, as shown in Figure 3. The aluminum plasmonic grating is placed inside a vacuum system at 10^{-6} Torr pressure, mounted on a copper stage that is thermally coupled to a liquid nitrogen bath outside the chamber. When the stage is cooled to 77 K, N_2H_4 vapor is introduced into the vacuum system. The chamber pressure is raised to 10^{-5} Torr by introduction of N_2H_4, and N_2H_4 molecules are adsorbed on the aluminum grating surface. An unpolarized, pulsed KrF laser operating at 10 $W\,m^{-2}$ at 248 nm and 1 Hz pulse rate is directed through a viewport into the vacuum chamber at normal incidence on the grating. The plasmonically enhanced optical field resonantly dissociates N_2H_4 molecules into dissociation products such as N_2H_3. The dissociation products are monitored via mass spectrometry with a filament at an ionization energy of 70 eV.

The mass spectrometry data from a typical experiment are shown in Table I. The left column lists the dissociation products of N_2H_4 that are detected by the mass spectrometer. In the middle two columns, we compare the partial pressure and quantum yield of the dissociation products from the aluminum grating substrate and a control substrate consisting of a quartz slide exposed to hydrazine under the same experimental conditions. The signal from each species, S_i, in the measured mass spectrum is a convolution of ions generated by resonant ultraviolet dissociation of N_2H_4, labeled S_{Li}, as well as species that are generated by gas phase N_2H_4 molecules that are dissociated by the mass spectrometer filament directly, labeled S_{Di}. To correct for mass signals that are not due to ultraviolet dissociation of hydrazine, the partial pressure and quantum yield are calculated according to the following procedure. First, the relative ratio of dissociated species is measured in the dark, defining S_{Di}. The corrected signal, S_{Li}, listed in Table I is obtained by subtracting the partial pressure of each dissociation product, S_i, from the partial pressure measured in the dark, S_{Di}, normalized for the total amount of N_2H_4 molecules that were ionized and detected

$$S_{Li} = S_i - \frac{S_{Di}}{\sum_i S_{Di}} \sum_i S_i. \tag{1}$$

We assume that the relative ratio of species generated only by the spectrometer filament, S_{Di}, does not change when the laser is on versus in the dark. Our mathematical procedure ensures that condensed N_2H_4 species on the plasmonic substrate that are released without undergoing ultraviolet dissociation, e.g., from heating or ablation, are not counted in the corrected yield. For each of the dissociated species, the quantum yield, QY_i, is determined from the partial pressure and calculated to be

$$QY_i = \frac{g * S_{Li}}{number\ of\ photons}, \tag{2}$$

This article is copyrighted as indicated in the article. Reuse of AIP content is subject to the terms at: http://scitation.aip.org/termsconditions. Downloaded to IP: 131.215.70.231 On: Tue, 20 Jan 2015 15:53:04

TABLE I. The corrected partial pressure and quantum yield of the dissociated N_2H_4 species based on mass spectrometry.

	Plasmonic substrate		Control substrate		
Dissociated species	Corrected partial pressure (10^{-9} Torr), S_{Li}	Quantum yield (10^{-4}), QY_i	Corrected partial pressure (10^{-9} Torr)	Quantum yield (10^{-4})	Enhancement ratio, R_i
N	0.3	4	0.008	1	3.6
NH_2	4.5	70	0.1	2	32.6
NH_3	4.1	60	0.2	4	17.6
N_2	3.0	40	1.4	20	2.1
N_2H	4.3	70	0.2	3	20.3
N_2H_3	1.9	30	0.4	6	5.0
Total	18.0	200	2.4	30	6.2 (R)

where g is a geometric factor relating partial pressure to absolute number of particles based on our chamber configuration. The right column of Table I shows the enhancement ratio, R_i, of each detected hydrazine decomposition product on the plasmonic substrate as compared with the products from the control substrate. Significantly, the plasmonic substrate enhances the dissociation of every species. The overall enhancement ratio R is calculated by taking the average of all enhancement factors for each dissociation product, where i and j are independent parameters

$$R = \frac{\sum_i R_i \frac{S_{NHi}}{2} + \sum_j R_j S_{N2Hj}}{\sum_i \left(\frac{S_{NHi}}{2} + S_{N2Hi} \right)}. \quad (3)$$

The total enhancement factor is 6.2× for all N_2H_4 dissociation products when using the plasmonic aluminum substrate compared with the quartz substrate.

In conclusion, we demonstrate a plasmonic nanostructure to concentrate ultraviolet radiation and enhance the generation of reactive nitrogen species athermally via resonant photodissociation by an overall factor of 6.2×. Surface plasmon-enhanced athermal dissociation processes, like those demonstrated here, may potentially open alternative pathways for the growth of nitride semiconductor films, by generating reactive nitrogen-containing precursors for film growth at low temperatures.

This work was supported by DARPA under Grant No. W911NF-13-1-0040 and utilized facilities of the Kavli Nanoscience Institute at Caltech.

[1]Y. K. Kuo, T. H. Wang, J. Y. Chang, and M. C. Tsai, Appl. Phys. Lett. **99**, 091107 (2011).
[2]O. Jani, I. Ferguson, C. Honsberg, and S. Kurtz, Appl. Phys. Lett. **91**, 132117 (2007).
[3]S. Strite and H. Morkoc, J. Vac. Sci. Technol., B **10**, 1237 (1992).
[4]T. Miyazaki, T. Fujimaki, and S. Adachi, J. Appl. Phys. **89**, 8316 (2001).
[5]F. K. Yam and Z. Hassan, Superlattices Microstruct. **43**, 1 (2008).
[6]M. A. Hoffbauer, T. L. Williamson, J. J. Williams, J. L. Fordham, K. M. Yu, W. Walukiewicz, and L. A. Reichertz, J. Vac. Sci. Technol., B **31**, 03C114 (2013).
[7]A. Kinkhabwala, Z. Yu, S. Fan, Y. Avlasevich, K. Mullen, and W. E. Moerner, Nat. Photonics **3**, 654 (2009).
[8]L. Brus, Acc. Chem. Res. **41**, 1742 (2008).
[9]C. J. Chen and R. M. Osgood, Phys. Rev. Lett. **50**, 1705 (1983).
[10]R. T. Kidd, D. Lennon, and S. R. Meech, J. Chem. Phys. **113**, 8276 (2000).
[11]S. Linic, P. Christopher, and D. B. Ingram, Nat. Mater. **10**, 911 (2011).
[12]S. M. Morton and L. Jensen, J. Chem. Phys. **135**, 134103 (2011).
[13]H. Nabika, M. Takase, F. Nagasawa, and K. Murakoshi, J. Phys. Chem. Lett. **1**, 2470 (2010).
[14]A. Nitzan and L. E. Brus, J. Chem. Phys. **75**, 2205 (1981).
[15]R. A. Pala, K. T. Shimizu, N. A. Melosh, and M. L. Brongersma, Nano Lett. **8**, 1506 (2008).
[16]M. Juan, M. Righini, and R. Quidant, Nat. Photonics **5**, 349 (2011).
[17]R. Bardhan, S. Lal, A. Joshi, and A. Halas, Acc. Chem. Res. **44**, 936 (2011).
[18]G. L. Vaghjiani, J. Chem. Phys. **98**, 2123 (1993).
[19]E. L. Woodbridge, M. N. R. Ashfold, and S. R. Leone, J. Chem. Phys. **94**, 4195 (1991).
[20]W.-G. Liu and W. A. Goddard, J. Am. Chem. Soc. **134**, 12970 (2012).
[21]Y. Watanabe, W. Inami, and Y. Kawata, J. Appl. Phys. **109**, 023112 (2011).
[22]M. W. Knight, L. Liu, Y. Wang, L. Brown, S. Mukherjee, N. S. King, H. O. Everitt, P. Nordlander, and N. J. Halas, Nano Lett. **12**, 6000 (2012).
[23]J. Hu, L. Chen, Z. Lian, M. Cao, H. Li, W. Sun, N. Tong, and H. Zeng, J. Phys. Chem. C **116**, 15584 (2012).
[24]M. A. Verschuuren, Ph.D. dissertation, Utrecht university, 2010.

This article is copyrighted as indicated in the article. Reuse of AIP content is subject to the terms at: http://scitation.aip.org/termsconditions. Downloaded to IP: 131.215.70.231 On: Tue, 20 Jan 2015 15:53:04